Experimental Astronomy manuscript No.
(will be inserted by the editor)

Electrical Interferences Observed in the Cassini CIRS Spectrometer

by Cheong Chan, Shane Albright, Nicolas Gorius, John Brasunas, Don Jennings, F. Michael Flasar, Ronald Carlson, Ever Guandique and Conor Nixon

Received: date / Accepted: date

Abstract The Composite Infrared Spectrometer (CIRS) carried onboard the Cassini spacecraft has now operated successfully for 17 years, following launch in 1997. Following insertion into Saturnian orbit in July 2004, the instrument has taken data nearly continuously, returning over 100 million interferograms (spectra) to date. Although of generally high quality, and resulting in more than 100 peer-reviewed scientific articles, the spectra are afflicted with several types of instrumental electrical (non-random) noise artifacts. These noise artifacts require either mitigation strategies (prevention), removal from the observed data, or else awareness of the affected spectral areas which must be excluded from scientific analysis. The sources and nature of these varied noise types were not readily identified until after launch. The purpose of this article is to inform users of the noise in the CIRS dataset and to serve as a 'lesson-learned' guide to pitfalls for designers of future instruments.

Keywords Fourier Transform Spectrometer · Electrical Noise · Engineering · Spacecraft Instrumentation

1 Introduction

The Cassini-Huygens unmanned spacecraft is the first, flagship-class robotic spacecraft sent into Saturn orbit to explore the planet, its rings and its moons. The mission is managed by the Jet Propulsion Laboratory and it is a product of the combined effort of NASA and the European Space Agency (ESA)(Matson et al. 2002). Launched in October 1997 on a Titan IVB with a Centaur upper stage, the Cassini-Huygens spacecraft arrived at Saturn in July 2004 and it is expected to continue to work through the solstice mission until 2017 (Fig. 1).

Cheong Chan
NASA Goddard Space Flight Center Bldg. 34
Tel.: +415-589-9697
E-mail: cheong.chan@yale.edu

The mission is made of two spacecraft: the Cassini orbiter and Huygens lander. The Huygens probe descended into Titan's atmosphere in January 2005 and was the first spacecraft to successfully land on a celestial body in the outer solar system (Lebreton et al. 2002). The orbiter, powered by three plutonium thermoelectric generators, has been hugely successful and its mission was extended several times after the primary mission ended in 2008.

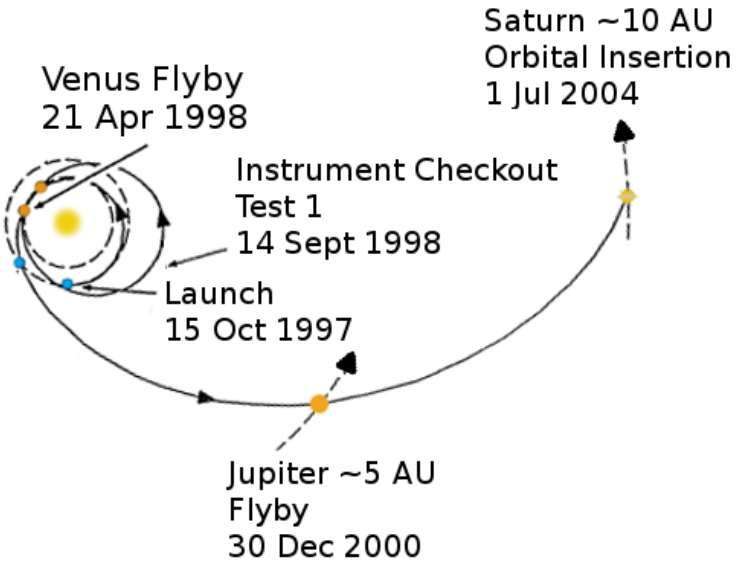

Fig. 1 Diagram of the flight trajectory timeline of Cassini space probe from launch until orbital insertion with relevant dates of testing indicated. This diagram is a modified version of one found in a paper describing the trajectory of the mission (Peralta et al. 1995)

One of the major science instruments on-board the Cassini orbiter is the Composite Infrared Spectrometer (CIRS). Using the data from CIRS, three dimensional maps of temperature, gas composition, and aerosols of the atmospheres of Jupiter, Titan, and Saturn can be created(Flasar et al. 2004a;b; 2005a;b; Hesman et al. 2009; Howett et al. 2007; Kunde et al. 2004). This information helps refine models of solar system formation and atmospheric dynamics of the gas giant and Titan (Flasar et al. 2004a; Nixon et al. 2007; Teanby et al. 2008; Vinatier et al. 2010). Some of the discoveries enabled by the CIRS instrument include the study of the 'tiger stripes' on Enceladus' south polar surface and the detection of propylene in Titan's atmosphere (Nixon et al. 2013; Spencer et al. 2006).

Due to the long development cycles of instruments on deep space missions, the changing media of the documentation, and flux of team members, the lessons learned from the design and operation of the instrument are often lost.

This paper is aimed towards preserving the lessons learned and the content should be accessible to anyone participating in the development of a similar future instrument. The organization of the paper is (i) a brief description of the instrument; (ii) a description of the non-random, electrical noise encountered during the mission; (iii) a discussion of the mechanical noise encountered during the mission; and (iv) a summary on areas of improvement for engineering future instruments to avoid these problems. Although rigorous ground-tests were carried out where some of the noise was detected, this paper will explain why its significance was not understood until CIRS measurements were taken in space. The description of the interferometer will include a simplified explanation of the basic operating principles of the instrument. The description of the non-random noise sources includes an explanation of the impact on the data, the underlying cause (where known), and the suppression strategy used by the team. This paper builds upon previous works such as (Carlson et al. 2009; 2011; Nixon et al. 2012) and additionally summarizes knowledge that was previously available only through internal documents.

2 CIRS Overview

The CIRS instrument is composed of two interferometers operating at a range of 10-600 cm^{-1} in the far infrared and a range of 600-1400 cm^{-1} in the mid-infrared using a single telescope and scan mechanism. It has a spectral resolution that can be set from 0.5 to 15.5 cm^{-1}. The far-IR interferometer is a Martin-Puplett design that uses two thermopile detectors in focal plane 1 (FP1). The mid-IR interferometer is a standard Michelson design that uses an array of HgCdTe photoconductive detectors that are sensitive to the range 600-1100 cm^{-1} in focal plane 3 (FP3) and an array of HgCdTe photovoltaic detectors that are sensitive to 1100-1400 cm^{-1} in focal plane 4 (FP4) (Brasunas et al. 2004; Flasar et al. 2004a; Kunde et al. 1996; Martin et al. 1969; Maymon et al. 1993; Nixon et al. 2009). In operation, the telescope is pointed toward the target of interest and the light collected is split between the two interferometers.

For each interferometer, the basic working steps are to: 1) split the input light into two paths (arms of the interferometer), 2) add a variable phase delay to one of the paths by making one arm longer, and 3) recombine the light on a detector. The amplitude of the light measured at the detector will be a function of the phase delay since the recombined light from the two paths can interfere (Griffiths et al. 2007). In the CIRS instrument, the phase delay is added via extra travel path of the light reflecting off the scan mirror pictured in the middle of (Fig. 2). The plot of the signal as a function of the delay distance is called the interferogram. For example, the light of a pure monochromatic signal would have an interferogram that looks approximately like a cosine function in an ideal interferometer. For a general source, the interferogram is the Fourier cosine transform of the power spectrum of the light for an ideal interferometer. The expression for the AC component of the intensity I in terms of the power

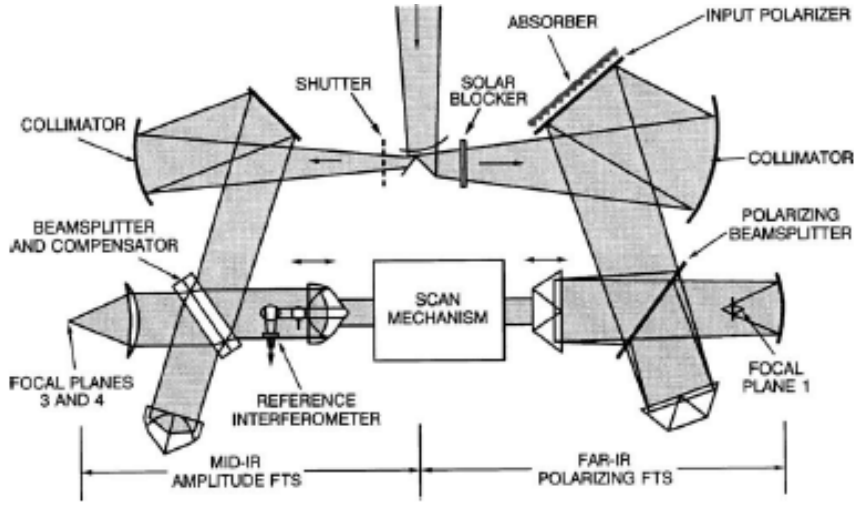

Fig. 2 This is a diagram of the basic optical layout of the CIRS instrument taken from (Kunde et al. 1996). The input light from the telescope at the top is split into the two interferometers whose path lengths are modified by a single scan mechanism. The light is directed to the three focal planes (detector arrays) as described in the text

spectrum for a given wavenumber $\tilde{\nu} = 1/\lambda$ and x (the distance of the mirror from a position where the arm lengths are equal) is given by:

$$I(x) = \int_0^\infty P(\tilde{\nu}) \cos(2\pi\tilde{\nu}x) d\tilde{\nu}. \quad (1)$$

For a delta function spectrum (monochromatic signal), the integral is simply the cosine factor evaluated where the argument of the delta function equals zero. The general name of this type of measurement scheme is called homodyne detection which uses an altered form of the original signal to mix the original signal to lower a high optical frequency to a detectable lower frequency. In the actual instrument, the non-ideal properties of the optical material as a function of wavelength and temperature can cause additional effects that must be compensated either by design or calibration. Since the scanning speed may not be exactly constant over the range of the scan, a laser is used to produce a comb for the detector to trigger measurements at very precise intervals of the delay length. For a more detailed description of the CIRS instrument, the reader should refer to the papers describing the instrument (Flasar et al. 2004a; Kunde et al. 1996).

The process for producing the interferogram is not finished until it is converted into digital information in memory on board the spacecraft. The analog signal from the detectors must undergo filtering, amplification and digitization on board the CIRS instrument electronics before being saved to memory. The noise we describe for the rest of the paper generally enter the signal in the conversion step.

3 Observed Electrical Interferences

In this section, we will discuss the non-random, electrical noises in the CIRS instrument identified by the CIRS team during the calibration process of the interferograms (Nixon et al. 2005; 2012). The calibration process occurred in space starting from the Instrument Checkout Test 1 and continued through the Jupiter flyby. For a detailed description of the random noises in the spectrometer such as Johnson noise or shot noise refer to the book by Hanel et al. (2003). The general layout of this section will be a description of the presence of the noise during the ground testing, a description of how the noise looks in the interferogram or spectrum (Fourier transformed space) of FP1, an explanation of the source, and strategies employed to suppress it. Table 1 provides a summary of these noise sources listed by their fundamental frequencies for reference. The main difficulty, which will be apparent for many of these noises, is the irregularity of the spike amplitudes or instability in frequency. This makes the removal of the noise during calibration a significant task. Throughout this section, we will use plots using sample number rather than wavenumber or Hz. The scan mechanism moves at a velocity of 0.0208 cm/s and the detector is triggered using a 783 nm laser zero-crossing with a decimation rate of 18 for FP1. Thus, the time spacing between each sample point is about 16.9 ms for a FP1 interferogram.

Table 1 A summary table of the fundamental frequency of noise sources

Frequency	Description and Location	Mitigation
1/2 Hz	Science Packet Collection FP1, and FP3	Shifted 5 ms per scan and software filtering
1 Hz	Analog Multiplexer FP1, and FP3	Randomized multiplexer readout timing
8 Hz	Spacecraft Communications Cycle FP1, and FP3	Shifted 5 ms per scan and software filtering
8 Hz	Internal Processing FP1, FP3, and FP4	Randomized processing schedule and software filtering
8.3 Hz	Unknown Source FP3	No mitigation
2-16 Hz	Sine Wave Noise FP1, and FP3	Software filtering under development

3.1 1/2 Hz Science Packet Collection and 8 Hz Spacecraft Communications

During the instrument checkout tests 1 starting on September 14, 1998, two patterns of noise appeared at quasi-regular intervals of the spacecraft clock in the FP1 interferograms. Both of these noise patterns are related to the communication cycles between the instrument and the spacecraft. The slower of these noise patterns had a .75 Hz fundamental frequency; this was changed to .5 Hz after the cooler cover release checkout with a flight software change (May 27, 2000). This lower frequency noise was determined to be related to the spacecraft querying science data from the instrument at 2 sec intervals.

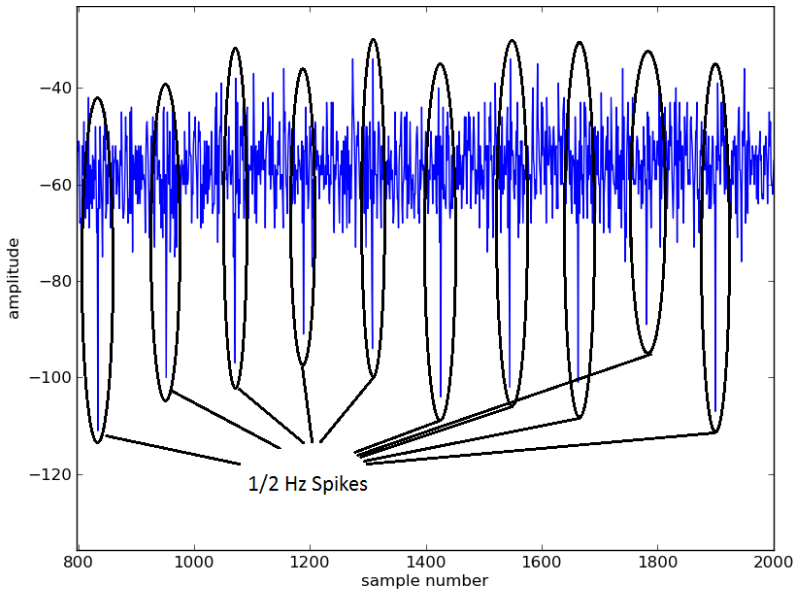

Fig. 3 Section of an interferogram of deep space from the detector at FP1 in a 50 sec scan with .5 Hz noise spikes (For a 50 sec scan there are about 2760 samples for a spacing of about 118 samples for .5 Hz). Deep space is shown due the simpler interferogram structure.

The other pattern is tied directly to the spacecraft clock which ticks at 1/8 of a second (1 Real Time Interrupt RTI). At 8 Hz, the spacecraft queries the instrument to check if there is a need upload any data (housekeeping, science, engineering). It is smaller than the 0.5 Hz spikes in (Fig. 3) and less apparent in the interferogram. The noise is best shown in the average of interferograms in (Fig. 4) and the spectrum in (Fig. 5).

The underlying cause of both these noises is attributed to power transients caused by sudden, increased loading on the BIU (Bus Interface Unit) during data communications between the instrument and the spacecraft. The control loop that maintains the power supply has a finite response time to changes in the current load. While the control loop is responding, the output capacitor

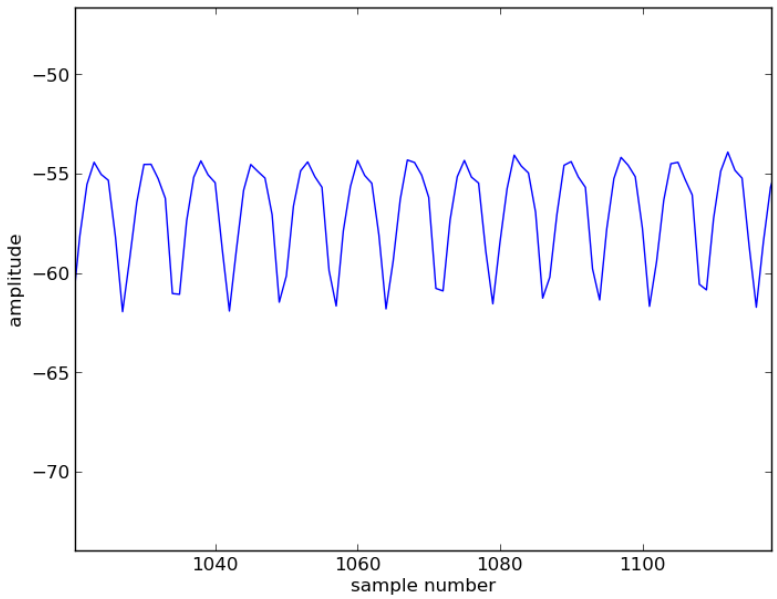

Fig. 4 Plot of an average of 6443 unfiltered interferograms of deep space showing the 8Hz noise from May 1, 2005 to Jun 21 2006 (number of sample points 2775-2785). The 1/2 Hz noise is suppressed on averages of greater than 16 spectra due to an update to the flight software on March 2005 where RTI scan lengths shifted to 16N+1 (where N is an integer).

is responsible for supplying the current to the load to compensate for the difference between the previous state and the new state (Texas Instruments 2007). Incorporation of a larger capacitor at the output of the regulator would suppress the transient (Fig. 6). As a work-around, the CIRS team mitigates the noise through flight software changes. This lack of ability to service the hardware highlights the special difficulty of space instruments compared to ones in the lab.

To suppress the effect of these noises in the flight software, the current strategy is to shift the beginning of the scan relative to the timing of the hardware by 5 ms per scan so that the spike pattern appears in different locations in different interferograms. This reduces the average noise amplitude at specific sample point positions for a mean of interferograms at the cost of increasing the average noise in other sample positions (Nixon et al. 2012). The noise spike can still be seen in each individual scan. It is essentially spreading the power of the noise over a larger spectral range. An additional post-process filtering is performed on each scan during the calibration of the data to further suppress the noise.

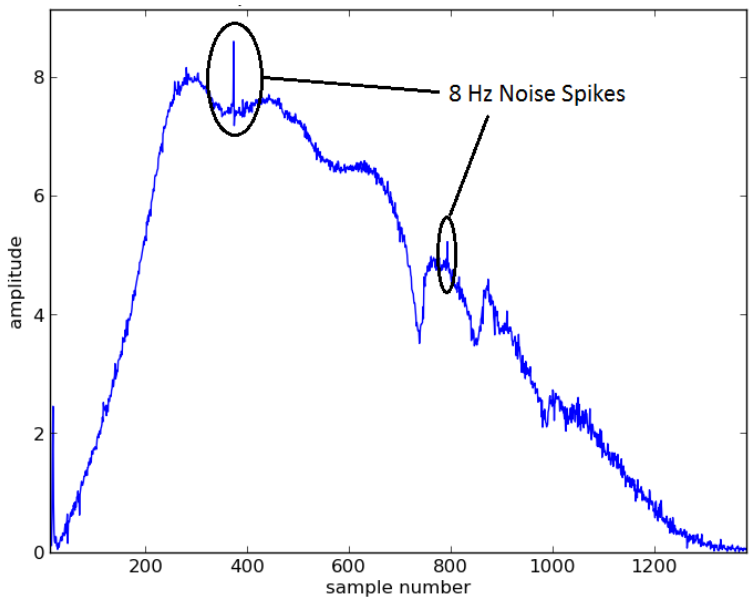

Fig. 5 Spectrum of the interferogram of deep space from FP1 in a 50 sec scan with 8 Hz noise spike at around sample number 400 and harmonic at sample number 800 (each sample number is 1/50 sec so an 8 Hz signal should be about 400). Additionally, the large spike at the low frequency end is the sine wave pattern and the pattern of smaller peaks at the beginning is the .5 Hz noise. Ideally, deep space should have a blackbody spectrum but the optics of CIRS add additional features.

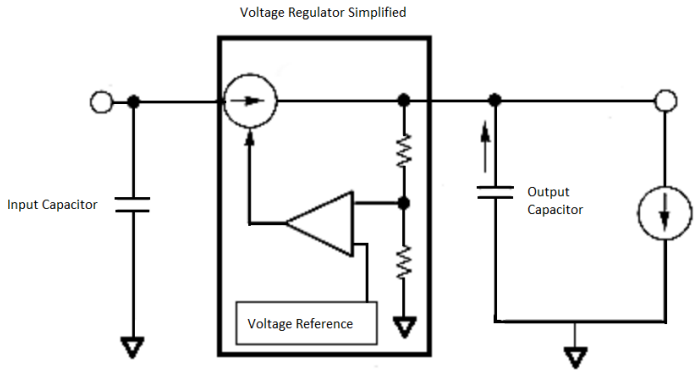

Fig. 6 This is a simplified schematic of a typical voltage regulator. When the load current is increased suddenly, the current is supplied by the output capacitor until the control circuit inside the regulator responds.

3.2 Internal Instrument Processing

This noise can be seen in all focal planes and it was first noticed during the investigation of the previously discussed noises. The instrument also uses the 8 Hz spacecraft clock for its own internal operations. Through experimentation, it was determined that this noise can be shifted by changing the timing of the instrument schedule of activities at each RTI such as: numerical filtering, data compression, packetization, etc. As of flight software version 6.0.0, the numerical filtering cycles are randomized to intervals between a range of 1 ms to 128 ms. Additionally, the noise shape changes when the other focal planes are not used. The underlying cause of this noise is similarly attributed to transients in the power supply due to the sudden loading of the BIU during the processing of the data. As the strategy to mitigate this is similar to the previous section, this does reduce the effect on an averaged spectrum, but an additional round of post-processing filtering is required to further suppress it.

3.3 Analog Multiplexer

A switching noise appears in the interferogram data in CIRS as a 1 Hz signal and it is the weakest of the electrical interferences (Nixon et al. 2012). The noise was discovered when a flight software change made the internal timing more tightly controlled, so as to avoid a timing conflict between two flight software tasks. This change caused the 1 Hz noise to no longer be pseudo-randomly averaged out over many scans. This noise is related to the analog multiplexer readout of the laser fringe voltage at one second intervals while science scanning is conducted.

An analog multiplexer is essentially an electronic switch that uses a digital signal to select an input from a set of inputs to output. They are typically used to reduce the number of components needed for the analog-to-digital (ADC) conversion required for the instrument. The engineering decision to use this design most likely stems from a need to save mass and power by reducing the number of ADC's. The analog multiplexers are placed after the sample and hold circuits but before the ADC stage in CIRS (Fig. 7).

These multiplexers can introduce transients when switching due to the output capacitance of the circuit (Fig 8). When the multiplexer switches channels, the accumulated charge in the capacitance of the switch needs to be discharged and the finite discharge time leads to transients in the output of the switch (Analog Devices 2009). This is the opposite problem of the power supply transients where lower output capacitance of the multiplexers would help the settling time. This noise was first suppressed by shifting the fringe voltage read timing into 8 preset delays. With the delays, the spikes' amplitude in the averaged interferogram is reduced. In flight software version 6.0.0, the spikes are suppressed by randomizing the delay timing of the fringe voltage read within a 254 ms range of time.

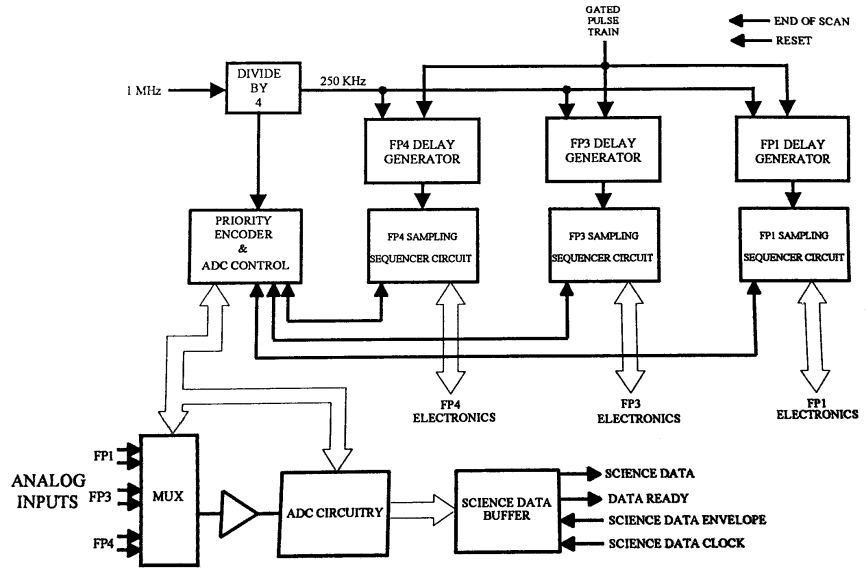

Fig. 7 This is a block schematic of the analog-to-digital converter circuit for the CIRS instrument contained on one of the instrument electronics boards. Flowing from lower left to lower right, the analog inputs come from the amplifiers of the detectors on each focal plane and feed into the analog multiplexer before being digitized (Barney et al. 1994).

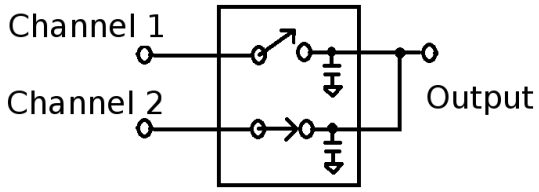

Fig. 8 Diagram of simplified circuit representation of analog multiplexer with switch capacitance shown in the box which must be discharged when the channel changes from the input on the left side from bottom to top.

3.4 Sinewave Noise FP1

The sine wave noise was first detected during the instrument checkout starting on September 14, 1998. Due to the low frequency and large amplitude of the noise at Cassini's Jupiter flyby, the noise can be seen by the naked eye in the interferogram (Fig. 9, 10). Unlike the previous noise sources where the timing is well controlled, this noise source is more variable in frequency and appears to have a high correlation to the electronics box temperature (Fig. 11). This appears as a linear relationship between the electronic box temperature and the frequency of the sine wave noise. The noise is approximately a sine wave

in the FP1 detector, but its frequency can change during the scan with the temperature.

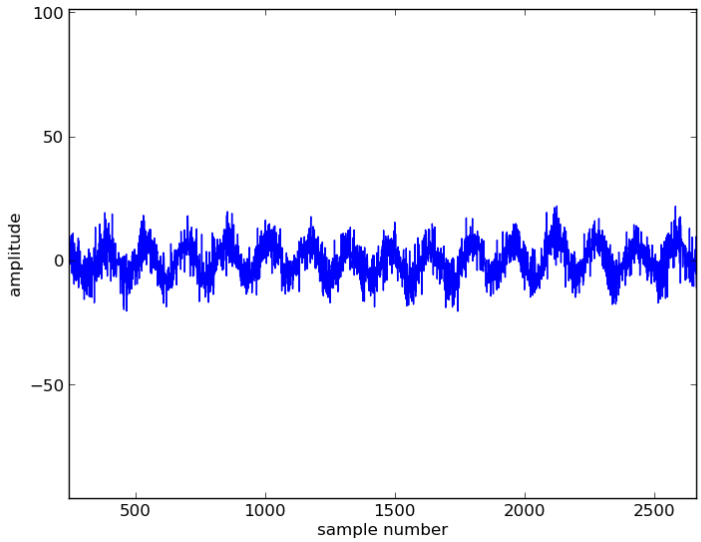

Fig. 9 Plot of an interferogram of a single scan of deep space when Cassini was close to Jupiter taken on Jan 2, 2001. The relatively low frequency sine wave noise is clearly seen.

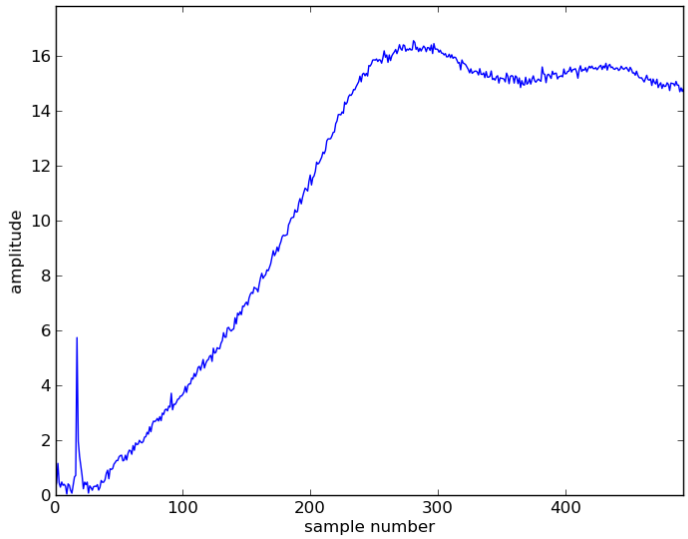

Fig. 10 Plot of the filtered power spectrum of a single scan of deep space taken on Jan 2, 2001. The sine wave noise appears as the large spike in the low sample number range.

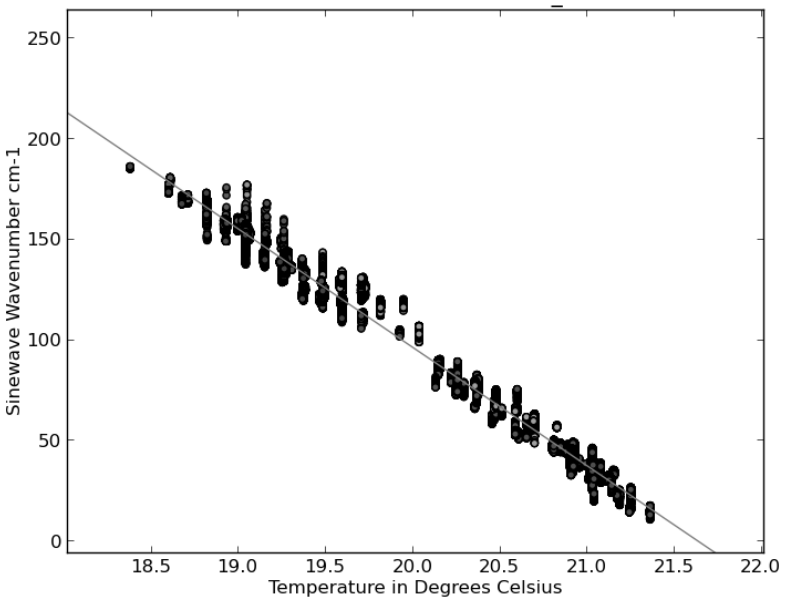

Fig. 11 The measured interference wavenumber for RTI ranges 200-420 from periods 01/2001-03/2001, 04/2004-06/2004, and 06/2006-09/2006 versus the temperature of the front end electronics sensor board 'c'. The temperature sensor has an accuracy of 100 mK and is regularly sampled by the instrument in 64 second intervals. Any values that fall in between are due to interpolation as the number of housekeeping samples are sparse compared to scans.

The resolution of the temperature measurement onboard the orbiter is limited and this implies that it cannot be used to accurately predict the wavenumber of the noise compared with the resolution of the instrument. The digitization of the temperature axis is clear in the spacing of the data points in (Fig. 11).

The fundamental cause of this noise is suspected to be the DC-DC switching power converters. They are chosen due to their much higher efficiency compared to linear regulators, but they operate at frequencies that are similar to the ADC frequencies in CIRS (Barney et al. 1994; Linear Technology 2013). The role is to convert the spacecraft bus voltage to a lower one for the instrument use. The tight power restriction is in turn due to the relatively small power source of the radioisotope thermoelectric generators of about 600 watts nominally. Although the converters are synchronized, it is likely the synchronizing oscillator is not locked to the presumably more stable ADC clock. In this case, temperature changes of the synchronizing oscillator would induce small frequency changes. The noise of the switching supplies could mix or alias with the similar operating frequency of the ADC to create an interference signal in the bandpass of the instrument. As the fundamental cause of this noise is not verified and it is uncertain whether there are readily available levers to

change this, the main strategy the CIRS team uses to deal with this noise is a post-process filtering step.

3.5 Suppression Results

In this section, we compare the results of the current mitigation strategies with no mitigation from earlier in the mission. The mitigation scheme depicted includes both the flight software version 6.0.0 and the post-processing in database version 3.2.1. The flight software incorporates the delay in timing of the scans described earlier and the post-process noise filtering is incorporated in the data product creation of the database v3.2.1. While the 8 Hz and .5 Hz noise still remain after averaging in the original detection scheme, the sine wave noise does average out (Fig. 12-13) and is mainly a concern during specific observation runs when it occurs on spectral features of certain molecules. With the mitigation scheme, the features due to the noise is greatly reduced in the average spectrum used for science (Fig. 14-15). Since the spikes still remain in each individual interferogram, they still contribute to the error associated with the mean interferogram.

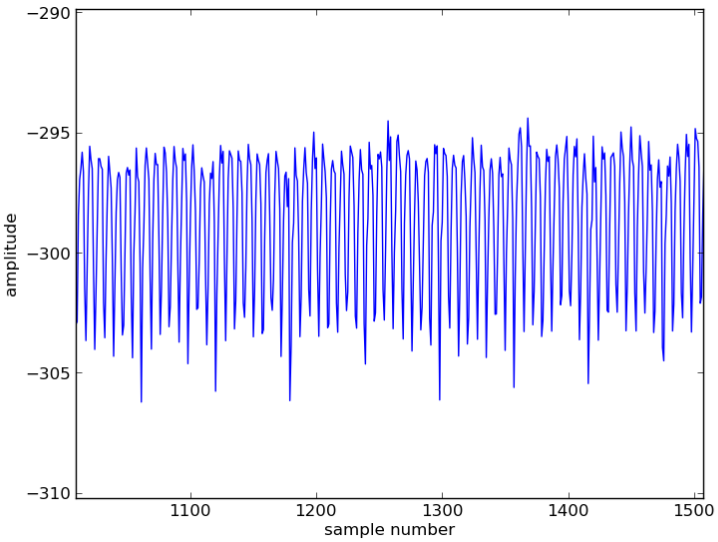

Fig. 12 This plot is an average of 254 Interferograms of deep space measured in Jan 2001. The large spikes are the .5 Hz noise and the smaller spikes are the 8 Hz noise.

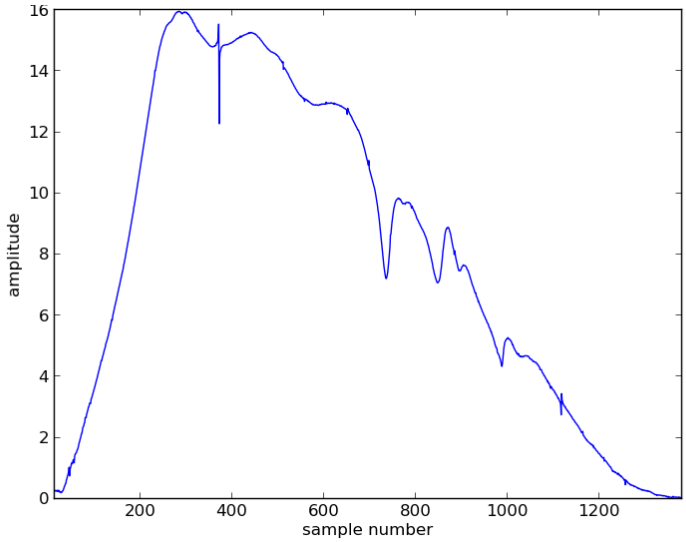

Fig. 13 This plot is a spectrum of an average of 254 Interferograms of deep space in Jan 2001. The large spike at 400 sample number is the 8 Hz peak.

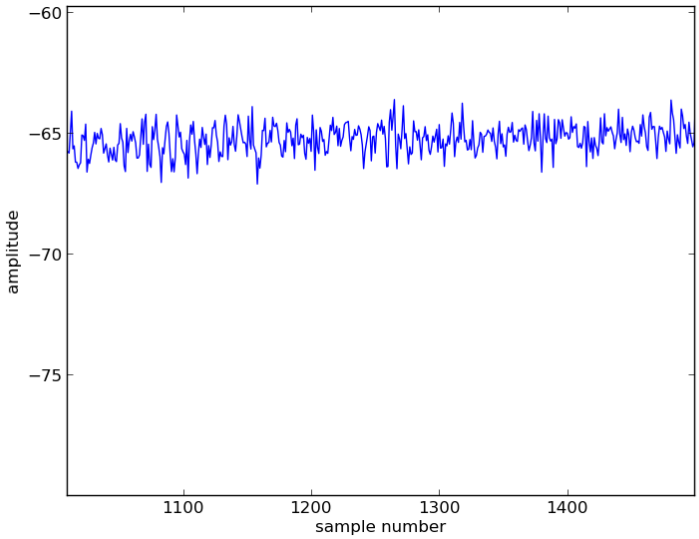

Fig. 14 Average of 254 Interferograms of deep space after change in flight software v6.0.0 and calibration database v3.2.1 measured in Jan 2011.

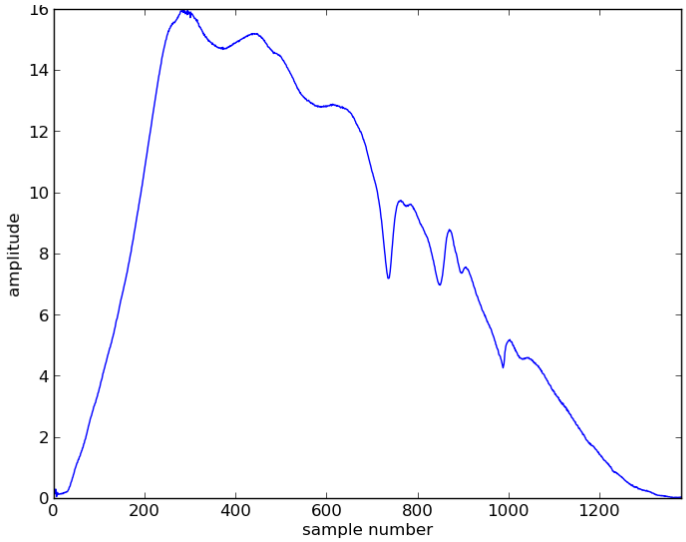

Fig. 15 Spectrum of average of 254 interferograms of deep space after change in flight software v6.0.0 and calibration database v3.2.1 measured in Jan 2011. The noise peaks are greatly reduced.

3.6 Ground Testing

The 8-Hz and 1/2-Hz spikes were not observed at Goddard because the spacecraft interface (BIU) simulator did not produce the same interrupt pattern as on the spacecraft. In the spacecraft ground integration tests at the Jet Propulsion Laboratory (JPL), the 8-Hz and 1/2-Hz were present, but the sensitivity of CIRS on the ground was not high enough to see them during the test. As a consequence, the CIRS team saw the noise during the first instrument checkout (ICO) in flight and the significance of the spikes which were present in the JPL spacecraft integration data was understood.

The ground EMI/EMC testing at the instrument level at Goddard and at the spacecraft level at JPL did not show the sinewave, presumably because the electronics temperature was higher than in flight and the frequency of the sinewave was close to zero (DC). It was not until Jupiter, when the electronics temperature began to decrease, that we found the sinewave. The sensitivity of CIRS improved by about a factor of two in the more benign electrical and vibration-free environment of space, making the sinewave more visible. The sinewave frequency continued to increase as Cassini moved on to Saturn.

Figure 16 is a sample CIRS FP1 noise equivalent spectral radiance. Figure 17 shows the ground testing setup. The three spikes at about 380, 440 and 505 cm-1 are the Mylar features, and their fine structure is likely due to sampling jitter. The feature at 190 cm-1 is at 8-hz, so it could be the BIU simulator and its width is probably due to sampling jitter. The environment was very noisy during chamber testing the CIRS team could not obtain a really good

spectra until after launch. This is a common problem with testing flight Fourier transform spectrometers on the ground.

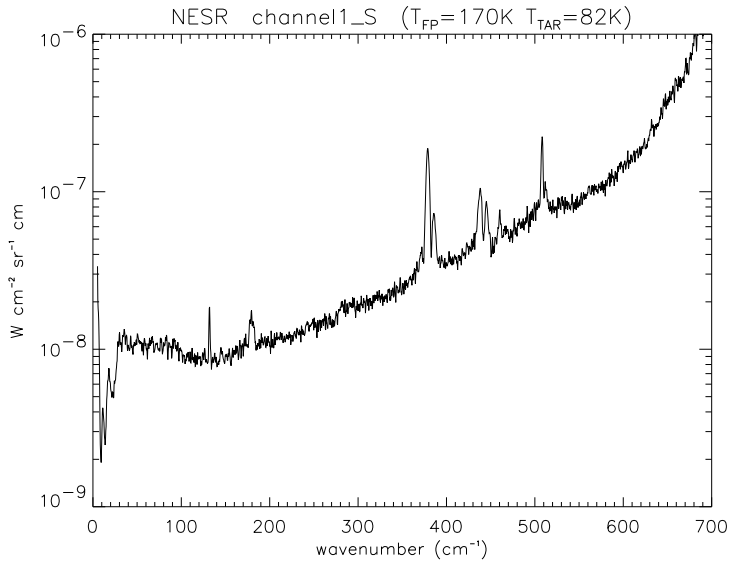

Fig. 16 CIRS FP1 noise equivalent spectral radiance measured at GSFC during ground testing on date August 13 with target temperature at 170K and detector temperature at 82K

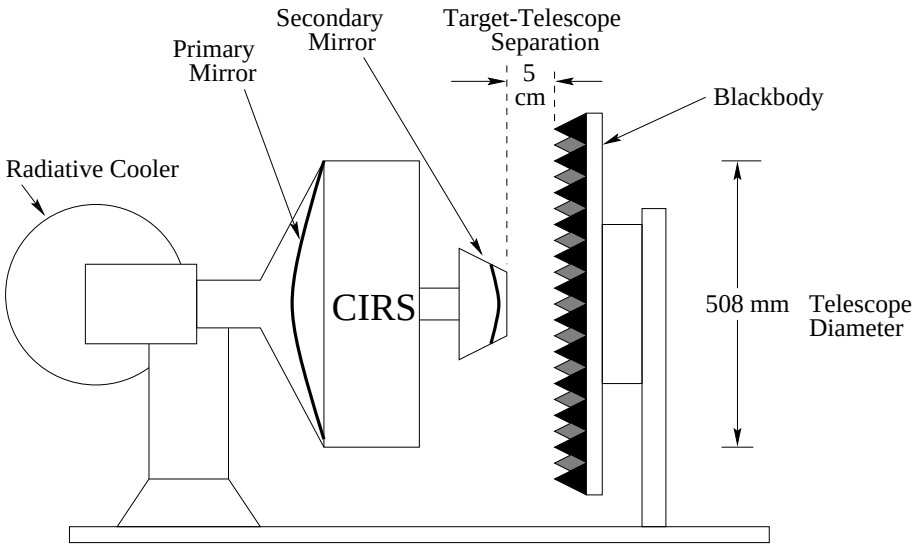

Fig. 17 Ground testing setup of CIRS with warm black body target.

4 Mechanical Noise Sources

Beyond purely electrical noise sources, there are mechanical noise sources that must be taken into consideration. One source of mechanical disturbance aboard the Cassini orbiter is the reaction wheels. A reaction wheel is essentially a flywheel driven by a DC motor that changes the rotational rate of the spacecraft through the conservation of angular momentum. Reaction wheels and small reaction control thrusters are responsible for the attitude control of the spacecraft and they are integral in the precise pointing of the spacecraft at the desired targets (Macala et al. 2014). Cassini started out with four reaction wheels with three needed to control each axis and a fourth to serve as a backup. From 2003, one of the main reaction wheels developed an anomalous instability and was replaced by the backup. Since then, the reaction wheels have continued to operate under careful management with some signs of aging appearing in the form of increased drag in the bearings. Due to the imperfect construction of the wheel assemblies, imbalances in the flywheel are the main cause of vibrations with a fundamental frequency at the rotation rate and this noise is a key concern for many optical instruments (Masterson et al. 1999). This vibration couples to the spacecraft and to the interferometer. In CIRS, the vibration disturbs the phase lock loop of the mirror scan mechanism that helps it maintain a constant scan velocity (Nixon et al. 2005). This noise was first discovered in data around 2004 during deep space scans. It was increasingly seen in target scans as the wheels aged and the mass distribution changed due to the detaching of the Huygens probe and fuel usage. The main strategy currently employed is to avoid the worst rates during observations where possible (Fig. 18).

In addition to the reaction wheels, the Low Energy Magnetospheric Measurement System of the Magnetospheric Imaging Instrument (MIMI) also contributed mechanical noise that could be detected on CIRS. It is essentially an actuating tube that accepts charged particles from a given direction and uses an array of detectors to discriminate the particle energy (Krimigis et al. 2004). The purpose of the instrument is to use the measurement of the particles to infer properties of the dynamics of the Saturn magnetosphere and its interactions with the solar wind. The instrument uses stepper motors to scan the field of view and to map out the population of the charged particles in the Saturn environment. The general advantageous characteristics of stepper motors are the ruggedness, high reliability/precision, and digital control of the motor. Unfortunately, the operation of the stepper motor in this instrument caused mechanical vibration in the spacecraft which in turn also caused phase lock loss in the scanning mechanism of the spectrometer (Nixon et al. 2005). This problem was resolved when the actuator was shut down in February 2005.

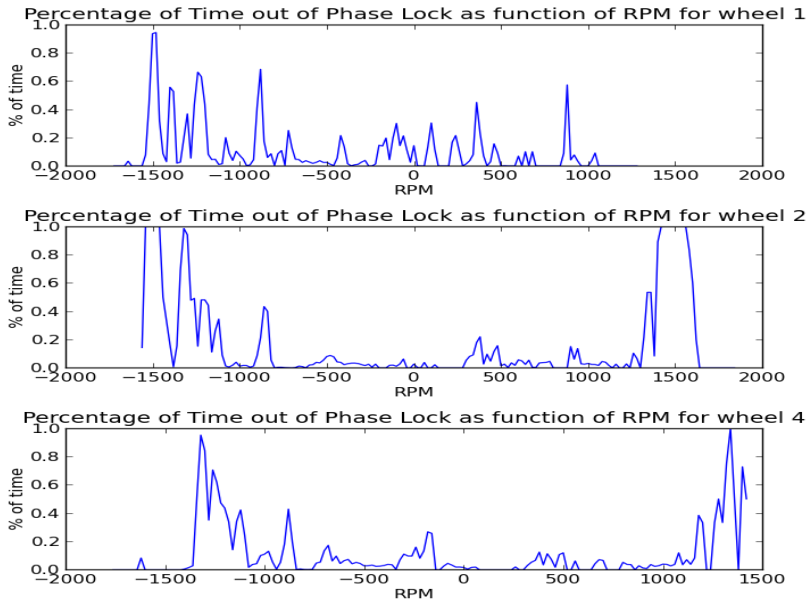

Fig. 18 These histograms indicates the percent of time the scan mechanism is out of phase lock as a function of reaction wheel spin rate expressed as rotations per minute (RPM). (data used from months 04/2004-05/2004 inclusively using all RTI values)

5 Future Recommendations for Design

For future instruments of this type, it is clear that a more conservative margin needs to be incorporated in the design of the detection to digitization electronics. In particular, the effect of transients due to additional loading from communications cycles and the use of multiplexers need to be more carefully considered. The majority of the noise spikes in CIRS could be suppressed if a more conservative filtering was introduced.

As a design can never perfectly match the operating conditions, additional features in the future electrical design could include re-writable EEPROM memory/FPGAs, fault handling, a debugging mode, and better housekeeping sensor resolution. With re-writable memory and FPGAs, the signal processing can be easily changed to handle unforeseen problems due to design or aging as repair operations are currently impossible. Due to the long communication cycle of the spacecraft, robust automatic fault handling that would log diagnostic information about the error and reset the instrument would decrease the loss of science data. A debugging mode that allows the collection of the raw data without any processing would aid in the identification of potential problems by decoupling noise introduced by the optics and spacecraft data processing. Lastly, better housekeeping measurements would allow for better

modeling of temperature effects and easier automatic detection of anomalies associated with operation through data mining (Takehisa et al. 2001). This detection would help operators identify potential problems more quickly.

For deep space missions, it is also recommended to add a control for the electronics temperature. This offers an additional degree of freedom to address problems such as the sinewave noise that may otherwise freely evolve as the instrument heats and cools. If such a control existed, the CIRS team could confirm the temperature dependence of the noise as the cause and shift the frequency to outside the bandwidth of interest.

In contrast to new features however, one recommended simplification to the design of the electronics would be to reduce the number of oscillators in the instrument to reduce the likelihood of interference. In CIRS, multiple similar oscillator frequencies is suspected to be cause of the sinewave interference.

In the mechanical design of the instrument, it is clear from past experience that there is a need of increased margin in vibration isolation. Due to the many potential sources of vibrational noise on the spacecraft, it is much easier to design additional isolation between the instrument and the spacecraft rather than hunting down and suppressing vibrational noise of every other part of the spacecraft. As with the electrical systems, more thorough integration testing of the completed spacecraft is important to verify of the spectrometer performance. This would mitigate potential design conflicts due to the finite scope of instrument and spacecraft subsystem teams.

Lastly, it is important to have accurate and readily available documentation of the current state of the instrument. Due to the long duration of the mission, the media of the documentation of the designs have greatly changed due to technological advances. Continued maintenance and updating of the formats of these resources is important due to the eventual need to go back to consult them later.

6 Conclusion

The CIRS instrument design has proven to be robust for having worked for almost two decades and it continues to be very successful in enabling scientific research. The key to success of this mission is the design simplicity and good communication of the requirements between the scientists and engineers. Additional features in future designs should be added with careful thought on the requirements as every addition grants one more failure mode. The goal of this paper is to review the major non-random noise sources of the CIRS instrument in order to improve the next generation of spectrometers. Experience points to the need to build in a little more margin to compensate for potential noise sources both external and internal to the instrument. For scanning Fourier transform spectrometers, an additional important aspect is the mechanical stability of the scanning mechanism; an extra margin of vibrational isolation between the instrument and the spacecraft can mitigate unforeseen noise originating from other parts of the spacecraft. Due to the current nature

of development and construction of large, deep space systems, these sort of subtler problems can best be mitigated through knowledge of past systems and extensive integration testing.

Acknowledgements The authors would like to thank the CIRS team for their cooperation and the NASA Education office for funding the internship.

References

Analog Devices "MT-088: Analog Switches and Multiplexers Basics" (2009)

Brasunas, J. C., and Lakew, B., "Long-term stability of the Cassini Fourier transform Spectrometer en route to Saturn", Recent Res. Devel. Optics, **4**, 95-113, (2004)

Carlson et al. "Characterization and Suppresion of Electrical Interference - Spikes, Periodic Waves, and Ripples - From Cassini Composite Infrared Spectrometer (CIRS) Spectra" in Advances in Imaging, OSA Technical Digest (CD) (Optical Society of America), paper FTuA5. (2009)

Carlson et al., Removing Artifacts in the Calibration of Cassini CIRS Spectra of Saturn and Titan, EPSC-DPS Joint Meeting, Nantes, France, 27 (2011)

Flasar et al., "Exploring the Saturn System in the Thermal Infrared: The Composite Infrared Spectrometer." *The Cassini-Huygens Mission* Springer (2004)

Flasar et al., "An intense stratospheric jet on Jupiter" Nature, **427**, 132-135 (2004)

Flasar et al., "Temperatures, Winds, and Composition in the Saturnian system" Science, **307**, 1247-1251 (2005)

Flasar et al., "Titan's Atmospheric Temperatures, Winds and Composition", Science, **308**, 975-978 (2005)

Barney et al., "Composite Infrared Spectrometer (CIRS) Critical Design Review Volume II", NASA Goddard Space Flight Center, (1994)

Griffiths, P., de Hasseth, J.A. *Fourier Transform Infrared Spectrometry* (2nd ed.). Wiley-Blackwell (2007)

Hanel, Rudolf A., ed. *Exploration of the solar system by infrared remote sensing.* Cambridge University Press, 260-264 and 277-278, (2003)

Hesman et al., "Saturn's latitudinal C2H2 and C2H6 abundance profiles from Cassini/CIRS and ground-based observations", Icarus, **202**, 249-259, (2009)

Howett et al., "Meridional variations in stratospheric acetylene and ethane in the southern hemisphere of the saturnian atmosphere as determined from Cassini/CIRS measurements", Icarus, **190** , 556572 (2007)

Krimigis et al., "Magnetosphere Imaging Instrument (MIMI) on the Cassini Mission to Saturn/Titan", Space Science Reviews, **114**, 233329 (2004)

Kunde et al., "Cassini Infrared Fourier Spectroscopic Investigation" *SPIE's 1996 International Symposium on Optical Science, Engineering, and Instrumentation.* International Society for Optics and Photonics, (1996)

Kunde et al., "Jupiter's Atmospheric Composition from the Cassini Thermal Infrared Spectroscopy Experiment." Science, **305**, 1582-1586 (2004)

Lebreton J. P., and Matson D. L., "The Huygens probe: science, payload and mission overview," Space Science Reviews **104**: 59100, (2002)

"Application Note 140," Linear Technology (2013)

Macala G. A., Lee, A. Y., and Wang E. K., "Feasibility Study of Two Cassini Reaction Wheel/Thruster Hybrid Controllers", Journal of Spacecraft and Rockets, **51**, No. 2, 574-585 (2014)

Martin, D. H., and Pulpett, E. "Polarised Interferometric Spectrometry for the Millimetre and Submillimetre Spectrum," *Infrared Physics*, **10**, 105-109 (1969)

Masterson, R. A., Miller, D. W., and Grogan, R., "Development of empirical and analytical reaction wheel disturbance models", AIAA Paper, 99-1204 (1999)

Matson, D. L., Spilker, L. J., Lebreton, J., "The Cassini/Huygens Mission to the Saturnian System," Space Science Reviews **104**, Issue 1-4, 1-58 (2002)

Maymon et al., "Optical Design of the Composite Infrared Spectrometer (CIRS) for the Cassini Mission" Proc. SPIE 1945 Space Astronomical Telescopes and Instruments II, **100** (1993)

Nixon et al., "Interferences on CIRS interferograms and Spectra: A User Guide," NASA GSFC (2005)

Nixon et al., "Meridional variations of C2H2 and C2H6 in Jupiter's atmosphere from Cassini CIRS infrared spectra" Icarus, **188**, 47-71 (2007)

Nixon et al., "Infrared limb sounding of Titan with the Cassini Composite InfraRed Spectrometer: effects of the mid-IR detector spatial responses," Appl. Opt. **48**, 1912-1925 (2009)

Nixon et al., "User Guide to the PDS Dataset for the Cassini Composite Infrared Spectrometer (CIRS)," NASA GSFC, (2012)

C. A. Nixon et al., "Detection of Propene in Titan's Stratosphere", ApJ **776** L14 (2013)

F. Peralta, S. Flanagan, Cassini interplanetary trajectory design, Control Engineering Practice, Vol. 3, Issue **11**, 1603-1610, (1995)

Spencer, J. R., et al. "Cassini encounters Enceladus: Background and the discovery of a south polar hot spot." Science 311.5766, 1401-1405 (2006)

Takehisa, Y., Kato, Y., and Hori, K., "Fault detection by mining association rules from house-keeping data.", Proc. of International Symposium on Artificial Intelligence, Robotics and Automation in Space., **3** No. 9. (2001)

Teanby et al., "Global and temporal variations in hydrocarbons and nitriles in Titan's stratosphere for northern winter observed by Cassini/CIRS", Icarus, **193**, 595-611 (2008)

Texas Instruments "AN-1733 Load Transient Testing Simplified", Application Report SNOA507 (2007)

Vinatier et al., "Analysis of Cassini/CIRS limb spectra of Titan acquired during the nominal mission. I: hydrocarbons, nitriles and CO2 vertical mixing ratio profiles", Icarus, **205**, 559-570, (2010)